JACS
JOURNAL OF THE AMERICAN CHEMICAL SOCIETY
Article
pubs.acs.org/JACS

Metal−Metal Bonding in Uranium−Group 10 Complexes

Johann A. Hlina,[†] James R. Pankhurst,[†] Nikolas Kaltsoyannis,*[,‡,§] and Polly L. Arnold*[,†]

[†]EaStCHEM School of Chemistry, University of Edinburgh, Joseph Black Building, The King's Buildings, Edinburgh EH9 3FJ, U.K.
[‡]Department of Chemistry, University College London, 20 Gordon Street, London, WC1H 0AJ, U.K.
[§]School of Chemistry, University of Manchester, Oxford Road, Manchester, M13 9PL, U.K.

Supporting Information

ABSTRACT: Heterobimetallic complexes containing short uranium−group 10 metal bonds have been prepared from monometallic $IU^{IV}(OAr^P\text{-}\kappa^2O,P)_3$ (**2**) $\{[Ar^PO]^-$ = 2-*tert*-butyl-4-methyl-6-(diphenylphosphino)phenolate$\}$. The U−M bond in $IU^{IV}(\mu\text{-}OAr^P\text{-}1\kappa^1O,2\kappa^1P)_3M^0$, M = Ni (**3−Ni**), Pd (**3−Pd**), and Pt (**3−Pt**), has been investigated by experimental and DFT computational methods. Comparisons of **3−Ni** with two further U−Ni complexes $XU^{IV}(\mu\text{-}OAr^P\text{-}1\kappa^1O,2\kappa^1P)_3Ni^0$, X = Me_3SiO (**4**) and F (**5**), was also possible via iodide substitution. All complexes were characterized by variable-temperature NMR spectroscopy, electrochemistry, and single crystal X-ray diffraction. The U−M bonds are significantly shorter than any other crystallographically characterized d−f-block bimetallic, even though the ligand flexes to allow a variable U−M separation. Excellent agreement is found between the experimental and computed structures for **3−Ni** and **3−Pd**. Natural population analysis and natural localized molecular orbital (NLMO) compositions indicate that U employs both 5f and 6d orbitals in covalent bonding to a significant extent. Quantum theory of atoms-in-molecules analysis reveals U−M bond critical point properties typical of metallic bonding and a larger delocalization index (bond order) for the less polar U−Ni bond than U−Pd. Electrochemical studies agree with the computational analyses and the X-ray structural data for the U−X adducts **3−Ni**, **4**, and **5**. The data show a trend in uranium−metal bond strength that decreases from **3−Ni** down to **3−Pt** and suggest that exchanging the iodide for a fluoride strengthens the metal−metal bond. Despite short U−TM (transition metal) distances, four other computational approaches also suggest low U−TM bond orders, reflecting highly transition metal localized valence NLMOs. These are more so for **3−Pd** than **3−Ni**, consistent with slightly larger U−TM bond orders in the latter. Computational studies of the model systems $(PH_3)_3MU(OH)_3I$ (M = Ni, Pd) reveal longer and weaker unsupported U−TM bonds vs **3**.

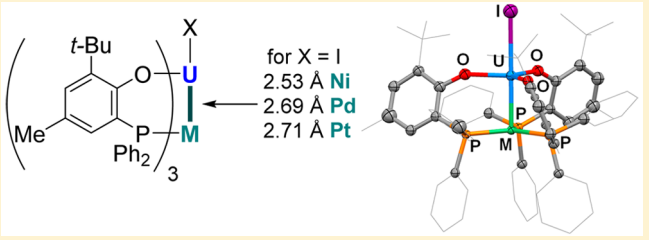

INTRODUCTION

The nature of the bonding in f-block metal−ligand bonds is still far from fully understood, and bonding between f-block metals and other metal cations even less so. By contrast, studies of the bonding between d-block and other metal cations are 50 years old and have furthered our understanding of d-orbital interactions and generated some unique small molecule activation chemistry and catalyzed reactions not seen in single metal chemistry.[1] The few complexes that feature bonds between an f-block and d-block cation[2−4] have begun to help to improve our understanding of metal−metal bonding and to challenge and help the development of computational methods; however, the challenges associated with their synthesis and characterization have precluded the systematic study of any families of heterobimetallics that would enable the prediction of trends in other systems. The 5f orbitals have a suitable spatial extension but not yet a predictability of participation in bonding that makes the d−f heterobimetallic bond a particularly interesting target to improve our understanding of the relative involvement of f- and d-orbital participation. A better understanding of the subtleties of the 5f/6d contributions to actinide bonding in general is important in the handling of nuclear materials, where differences in behavior are dominated by small covalency differences in bonding.

Compounds with a uranium−transition metal bond are limited to iron,[5−7] ruthenium,[5,8] cobalt,[9−11] rhenium,[12−14] and silver.[15] The first pair, $Cp_3U\text{-}MCp(CO)_2$ (M = Fe, Ru), was reported in 1987,[5] prepared via salt metathesis from Cp_3UCl and $Na[MCp(CO)_2]$. The investigation confirmed the presence of a metal−metal bond rather than an isocarbonyl bridge, but without crystallographic data, further analyses were difficult. We were able to isolate and structurally confirm the stable lanthanide analogue, $(L)(N'')NdFeCp(CO)_2$ [L = $Bu^tNCH_2CH_2\{C(NCSiMe_3CHNBu^t)\}$; N″ = $N(SiMe_3)_2$], the first complex with an unsupported 4f−3d metal−metal bond.[16] Liddle and co-workers translated this chemistry back to a uranium-supported bond by the tris(amido) tren framework[17] and extended the range of unsupported uranium−transition metal complexes further to cobalt and rhenium.[8,9,12−14]

Complementary to unsupported f/d-block metal bonds, which intrinsically rely on a negatively charged, ligating d-block

Received: October 13, 2015

DOI: 10.1021/jacs.5b10698
J. Am. Chem. Soc. XXXX, XXX, XXX−XXX

fragment, bridging ligands can provide more robust molecules. The Group 10 metal−thorium derivatives $(Cp^*)_2Th(\mu\text{-}PPh_2)_2Ni(CO)_2$ and $(Cp^*)_2Th(\mu\text{-}PPh_2)_2PtPMe_3$ ($Cp^* = C_5Me_5$) have unusual geometries and short Th−M distances of 3.206(2) and 2.984(1) Å, respectively,[18,19] the latter being described by calculations as a donor−acceptor bond from the pseudotrigonal-bipyramidal M^0 to the redox-inactive Th^{IV} center.

The groups of Bart and Thomas reported uranium−cobalt compounds with bridging heterobidentate monoanionic PN ligands.[10] At 2.874(3) Å, $ICo(\mu\text{-}Ph_2PNPr^i\text{-}\kappa^1P,\kappa^1N)_3UI$ (**A**) exhibits the shortest uranium−transition metal bond reported prior to this study; in this most instructive work, the analogue with Pr^i_2PNMes ligands (Mes = $C_6H_2Me_3$-2,4,6) was proposed from voltammetric experiments to have a stronger Co → U dative interaction than the relatively modest one in **A**, although the changes at both ends of the bidentate ligand make the components difficult to separate, and the latter complex was not structurally characterized. One of the arguments for using heterobidentate ligands has been to expand the variety of synthetic routes to M−M′ bonds; the photolytic release of CO from the isocarbonyl U−OC−Co moiety upon photolysis is arguably the most inventive synthesis yet, forming a 3.0319(7) Å U(IV)−Co(I) bond within the rigid NP scaffold $N[o\text{-}(NHCH_2PPr^i_2)C_6H_4]_3$ and with the suggestion of a close contact between the U center and another Co-bound CO ligand, while vibrational data suggest stronger donation of Co electron density to uranium through the bond than through the original isocarbonyl link, although the coordination of additional phosphines has also changed the ancillary ligand set somewhat.[11]

For comparison, the shortest distance yet found between an f and a d block metal is in the lutetium−platinum complex $(C_5Me_4SiMe_2CH_2PPh_2)Lu(\mu\text{-}CH_2SiMe_2CH_2)(OC_4H_8)PtMe_2$, 2.7668(5) Å,[20] which shows interesting intramolecular C−H bond cleavage chemistry at elevated temperatures.

Even though the heterobimetallic chemistry of rare-earth transition-metal compounds has now begun to receive considerable attention, examples with late transition metals are still rare.[2−4] Roesky also used phosphinoamido ligands to combine palladium with yttrium and lutetium in bi- and trimetallic compounds with 2.9898(6) Å (Y−Pd), 2.9712(8) Å (Lu−Pd), and 3.141(13) Å ($Y-Pd_2$) bond lengths for the trimetallic compound.[21]

We have targeted phosphine-functionalized aryloxide analogues of $U(IV)(OAr)_3X$ (OAr = 2,6-di-*tert*-butylphenoxide) first reported in the 1980s, anticipating binding of a second metal by the incorporated phosphine groups, and since then work by others and us has shown that the U−OAr bonds are sufficiently robust to allow many X-substitution reactions without ligand scrambling that can dominate f-block coordination chemistry.[22−27] Other robust ligand sets, such as bis(permethylcyclopentadienyl) or polydentate chelates, can be insufficiently mobile to allow the M−M′ distance to change according to metal size or electronic preference. We also considered that the X ligand in the trans position to a ligated metal ion would provide the possibility to exploit the inverse trans influence (ITI) in the formation of stronger bonds to an atom (here the second metal) in the position trans to X, the phenomenon whereby mutually trans-ligands bind closer and more tightly to a uranium center than they would in a d-block system, since the available (pseudocore) U 6p orbitals can mix with the valence 5f.[28−31]

We present a set of new heterobimetallic uranium−group 10 metal complexes using these simple ligands, the first study of an actinide−M bond for a complete transition-metal group and the first set of differently trans-ligand-functionalized uranium−metal bonds. We show how the ligand supports the shortest 5f−*n*d metal−metal bonds yet stabilized and preserves the metal−metal bond while allowing steric/electronic variation of the metal-bound X-ligand. These features have enabled a thorough study of the electronic structure of the metal−metal bond and its variation from 3d to 5d, and with ancillary ligand, for the first time.

SYNTHESIS

Preparation of the Ligand and Monometallic Compounds. The base-free potassium salt of the heterobidentate ligand 2-*tert*-butyl-4-methyl-6-(diphenylphosphino)phenolate (**1**, $KOAr^P$) may be prepared by deprotonation of 2-*tert*-butyl-4-methyl-6-(diphenylphosphino)phenol[32] in THF with KH.

The reaction of 3 mol equiv of **1** with uranium(IV) iodide etherate in THF gives $IU(OC_6H_2\text{-}6\text{-}Bu^t\text{-}4\text{-}Me\text{-}2\text{-}PPh_2\text{-}\kappa^2O,P)_3$ [$IU(OAr^P\text{-}\kappa^2O,P)_3$, **2**] as a bright green powder in 78% yield (Scheme 1).[25] Compound **2** is moderately soluble in benzene

Scheme 1. Synthesis of Uranium(IV) Tris(aryloxide) Iodide 2

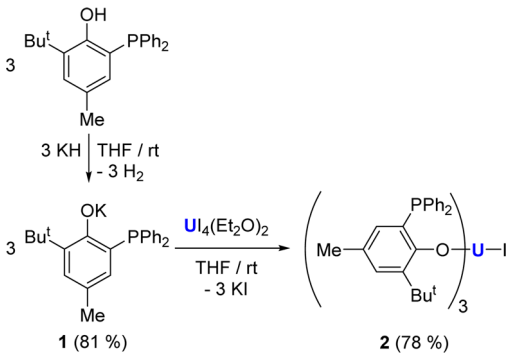

and toluene; ^1H NMR spectroscopy shows broad overlapping resonances at ambient temperature but seven resonances at elevated temperatures, although even at 370 K these are still broad. No ^{31}P NMR resonance is observed at 300 or 370 K, similarly to other uranium phosphine complexes, e.g., $U(dmpe)_2X_4$ (X = Cl, OPh, Me).[33,34] This could indicate a persistent coordination of the phosphine groups to the paramagnetic uranium or a more dynamic process that broadens the resonances to baseline. The room-temperature magnetic moment (Evans' method) of **2** is 2.4 μ_B.

Green crystals of **2** suitable for single-crystal X-ray diffraction were grown from a benzene solution at ambient temperature. The solid-state structure shows a coordination number of 7 for the uranium center with three bidentate phosphino-aryloxides (Figure 1). The U−O and U−I distances (ranging from 2.150(3) to 2.162(3) and 3.0414(6) Å, respectively) are slightly longer than those previously reported for $IU(OC_6H_3\text{-}2,6\text{-}Bu^t_2)_3$ [U−O, 2.092(8)−2.114(11) Å; U−I, 3.011(2) Å].[24] The difference is probably due to the three additional phosphine donor atoms in **2**. The U−P bonds lie between 3.041(1) and 3.056(1) Å. To the best of our knowledge there are no other examples of triarylphosphine uranium complexes; hence, a comparison is limited to the few crystallographically charac-

DOI: 10.1021/jacs.5b10698
J. Am. Chem. Soc. XXXX, XXX, XXX−XXX

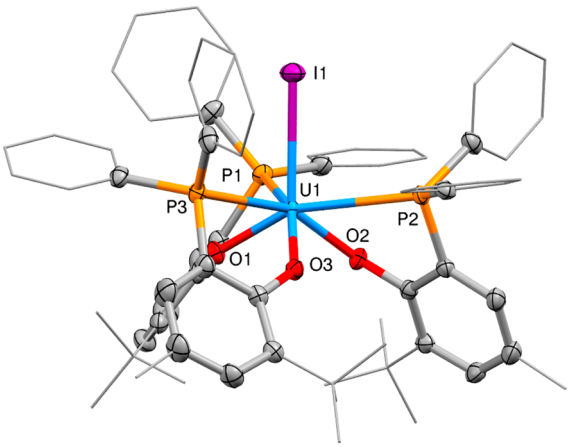

Figure 1. Molecular structure of **2**. Solvent molecules and hydrogen atoms are omitted, and peripheral carbon atoms are depicted as a wireframe, for clarity. Thermal ellipsoids are drawn at 50% probability. Selected distances (Å) and angles (deg): U−I, 3.0414(6); U−O, 2.150(3)−2.162(3); U−P, 3.041(1)−3.056(1); O−U−P, 62.93(8)−63.14(8); O−U−I, 79.98(2)−82.43(2), 119.43(8)−124.53(8).

terized trialkylphosphine uranium compounds. The U−P bond distances in **2** are similar to those of $U(dmpe)_2X_4$ (X = Cl, OPh, Me).[33,34] The related $U(IV)(Pr_2^iPNMes\text{-}\kappa^2P,N)_3UI$ has U−P distances between 2.8662(12) and 2.8828(4) Å.[10]

Preparation of the Bimetallic Compounds. The reaction of **2** with low oxidation state group 10 metal compounds incorporates the respective metal through phosphine ligation. The uranium(IV)−nickel(0) derivative is prepared by treatment of **2** with an equimolar amount of $Ni^0(cod)_2$ (cod = 1,5-cyclooctadiene) in toluene at ambient temperature (Scheme 2). An immediate color change to dark red indicates fast displacement of cod by the triarylphosphine donor groups. The new heterobimetallic $IU(\mu\text{-}OAr^P\text{-}1\kappa^1O,2\kappa^1P)_3Ni$ (**3−Ni**) is isolated as dark red crystals in excellent yield and exhibits similar solubility to the parent compound **2**.

Scheme 2. Preparation of the Bimetallic Uranium(IV) Complex 3−Ni, 3−Pd, and 3−Pt

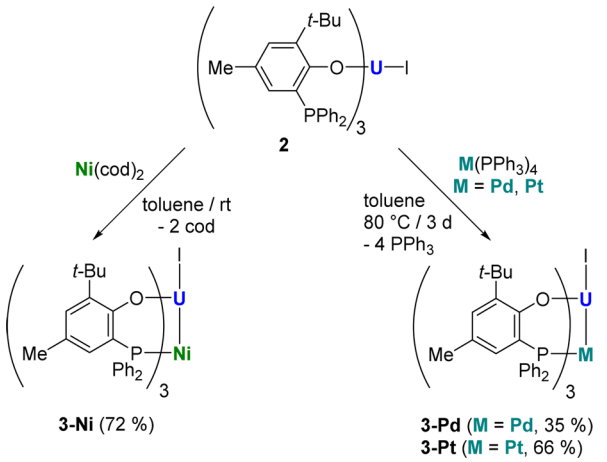

For the preparation of the heavier congeners, palladium(0) and platinum(0) phosphines proved to be suitable precursors, whereas $Pd_2(dba)_3$ (dba = dibenzylideneacetone) was unsuitable due to the ketone functional group [see the Supporting Information (SI)]. Reactions between equimolar amounts of **2** and tetrakis(triphenylphosphine)M(0) (M = Pd, Pt) in toluene at 80 °C give the bimetallic uranium(IV)−palladium(0) complex $IU(\mu\text{-}OAr^P\text{-}1\kappa^1O,2\kappa^1P)_3Pd$ (**3−Pd**) and uranium(IV)−platinum(0) complex $IU(\mu\text{-}OAr^P\text{-}1\kappa^1O,2\kappa^1P)_3Pt$ (**3−Pt**), respectively (Scheme 2). All three bimetallic complexes **3−Ni**, **3−Pd**, and **3−Pt** show remarkable thermal stability.

Upon introduction of the group 10 metal centers, the magnetic moment decreases from 2.4 μ_B in **2** to 1.9 μ_B (**3−Ni**), 1.8 μ_B (**3−Pd**), and 2.0 μ_B (**3−Pt**), respectively. The similarity of the values for the bimetallic systems might indicate analogous interaction between the different d^{10}-metals and uranium. However, a comparison of this group trend with previously reported systems is not possible, since no magnetic data were given for the only pair of complexes in which the ligand system remained unchanged between different transition-metal derivatives, $Cp_3UMCp(CO)_2$ (M = Fe, Ru).[5] Our observation contrasts with that of the groups of Bart and Thomas and of Arnold and Lu, who reported an increase of the magnetic susceptibility after introduction of the cobalt center into the amidophosphine-ligated uranium compounds.[10,11]

Single crystals suitable for X-ray diffraction studies of the bimetallic compounds were grown at ambient temperature by vapor diffusion of hexane into benzene solutions. The solid-state structures of the bimetallic complexes **3−Ni**, **3−Pd**, and **3−Pt** are similar and are shown in Figure 2. Selected distances and angles are collected in Table 1, along with the data from the DFT calculations described below. The agreement between experiment and theory is very good.

Despite the C_3-symmetry of the individual molecules, the structures of **3−Ni** and **3−Pt** could be refined only in the triclinic space group *P*1. The asymmetric unit of each contains nine molecules of the compound along with three benzene molecules each. The individual molecules show slightly different orientations and could not be refined using a space group of higher symmetry. Complex **3−Pd** was solved and refined in the trigonal space group $P3_2$ and contains three molecules of complex, with three benzene molecules per complex, in the asymmetric unit. The U−M bond distances increase from 2.527(2)−2.540(2) Å in **3−Ni** to 2.686(2)−2.694(1) Å in **3−Pd** and 2.706(1)−2.709(1) Å in **3−Pt** (Figure 2). The intermetallic bond distances are significantly shorter than those of any other crystallographically characterized d- and f-block bimetallic compound previously reported. [The shortest, Lu−Pt, noted above, is 2.7668(5) Å.[20]] The only other actinide−group 10 derivatives reported are $Cp^*Th(\mu\text{-}PPh_2)_2Ni(CO)_2$ and $Cp^*Th(\mu\text{-}PPh_2)_2PtPMe_3$, featuring intermetallic distances of 3.206(2) and 2.984(1) Å, respectively.[18,19] To the best of our knowledge, no other uranium−group 10 derivatives have been reported; comparison with the bimetallic $U^{IV}-Co^I$ $ICo(\mu\text{-}Ph_2PNPr^i\text{-}1\kappa^1P,2\kappa^1N)_3U[\eta^2\text{-}Ph_2PNPr^i]$ and $ICo(\mu\text{-}Ph_2PNPr^i\text{-}1\kappa^1P,2\kappa^1N)_3UI$ reported by the groups of Bart and Thomas is most instructive.[10] The short intermetallic bonds are accompanied by U−M−P bond angles larger than 90°: 91.7(1)−94.3(1)° (**3−Ni**), 90.36(9)−92.68(8)° (**3−Pd**), and 91.11(7)−93.57(7)° (**3−Pt**). The increase in U−M bond length caused by the increased atomic radius in the series from nickel to platinum appears to be compensated by a decrease in O−U−M−P torsion angle, leaving the anionic ligand sphere around the uranium centers virtually unaffected.

The U−I bonds of **3−Ni**, **3−Pd**, and **3−Pt** are shorter than those in the parent monometallic derivative **2** by around 0.04 Å in all cases. It is tempting to attribute this to the ITI. However,

DOI: 10.1021/jacs.5b10698
J. Am. Chem. Soc. XXXX, XXX, XXX−XXX

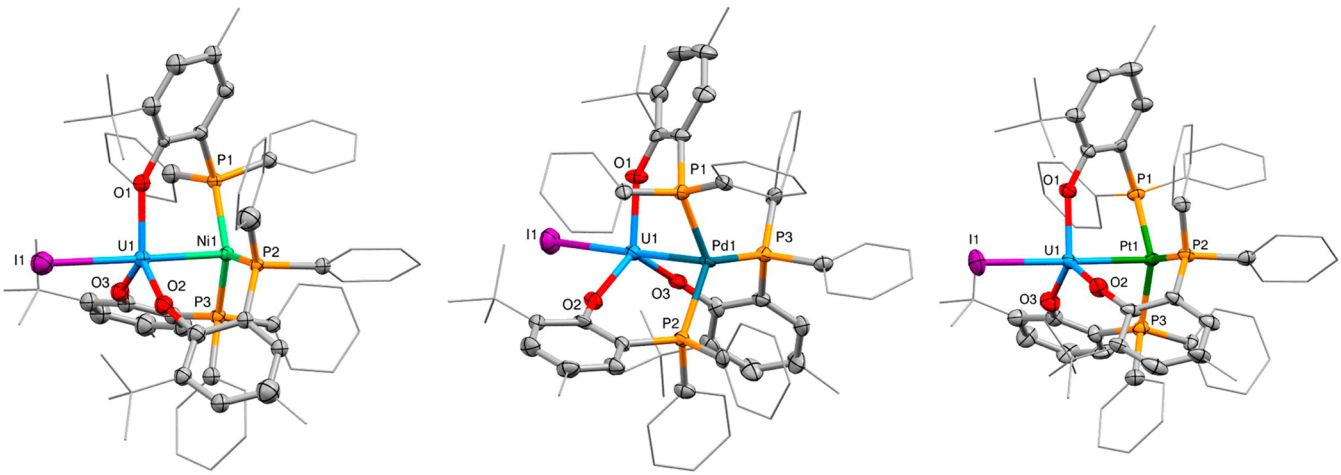

Figure 2. Thermal ellipsoid plot for **3−Ni**, **3−Pd**, and **3−Pt**. Solvent molecules and hydrogen atoms are omitted, and selected carbon atoms are depicted as a wireframe, for clarity. Thermal ellipsoids are drawn at 50% probability, and only one independent molecule out of nine in the asymmetric unit is shown. Selected bond distances (Å) and angles (deg) are shown in Table 1.

Table 1. Selected Bond Distances (Å) and Angles (deg) of the Solid-State Structures of 3−Ni, 3−Pd, and 3−Pt and the Calculated Values, Respectively[a]

	3−Ni		3−Pd		3−Pt
	expl	calcd	expl	calcd	expl
U−M (Å)	2.527(2)−2.540(2)	2.534	2.686(2)−2.694(1)	2.701	2.706(1)−2.709(1)
U−I (Å)	3.007(1)−3.012(1)	3.008	2.994(1)−3.007(1)	3.014	3.007(1)−3.014(1)
U−O (Å)	2.134(8)−2.16(1),	2.166 (av)	2.12(1)−2.14(1)	2.162 (av)	2.125(5)−2.15(1)
M−P (Å)	2.222(5)−2.239(4)	2.264 (av)	2.361(3)−2.368(3)	2.396 (av)	2.320(4)−2.330(3)
I−U−M (deg)	178.94(5)−179.58(6)	178.0	178.90(5)−179.34(4)	178.3	178.80(3)−179.13(3)
U−M−P (deg)	91.7(1)−94.3(1)		90.36(9)−92.68(8)		91.11(7)−93.57(7)
O−U−M−P (deg)	26.4(3)−31.8(3)		25.3(2)−30.2(2)		24.6(2)−29.3(2)

[a]Torsion angles are given for oxygen and phosphorus atoms bound to the same bridging ligand.

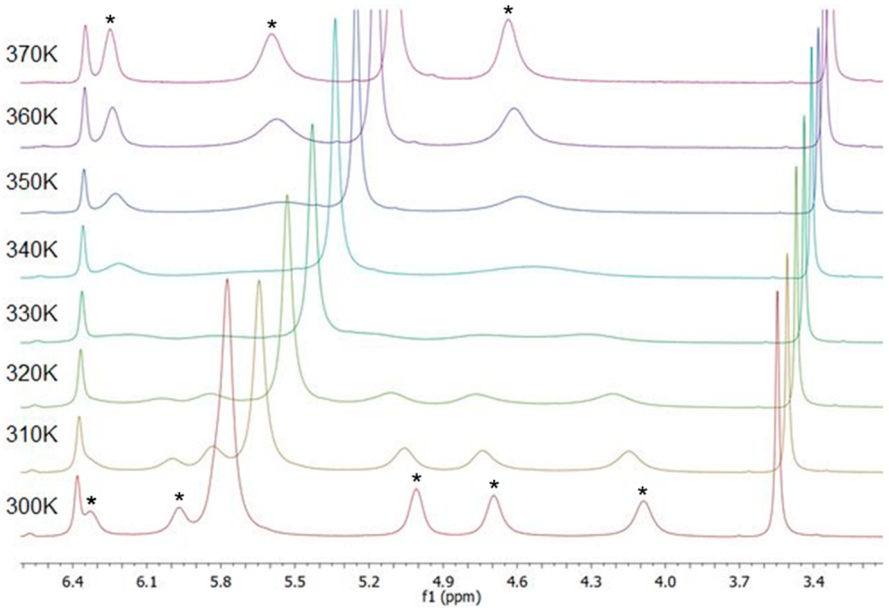

Figure 3. Stacked variable-temperature ^{1}H NMR spectra of **3−Ni** in toluene-d_8 from 3.2 to 6.6 ppm over a temperature range of 300−370 K. Asterisks indicate resonances of phenyl hydrogen atoms observable at 300 and 370 K.

it could simply be a result of the lower coordination number in the bimetallic complexes (5-coordinate at U, including the M−M bond) compared to the phosphine-ligated parent compound (7-coordinate at U) since the effective ionic radius of the 5-coordinate U will be up to 0.1 Å smaller.[35]

The compounds **3−Ni**, **3−Pd**, and **3−Pt** show paramagnetically shifted ^{1}H NMR resonances in the range 3.56−11.82 ppm

DOI: 10.1021/jacs.5b10698
J. Am. Chem. Soc. XXXX, XXX, XXX−XXX

(**3−Ni**), 5.32−15.44 ppm (**3−Pd**), and 1.99−10.95 ppm (**3−Pt**). Again, the C_3-symmetry of the solid-state structures is evident in solution, but the interconversion of the Δ and Λ isomers can now be observed using variable-temperature (VT) NMR spectroscopic experiments in the range 300−370 K (Figure 3 for **3−Ni**), with coalescence relating to the interconversion shown in Figure 4, which requires the breaking of the U−M bond.

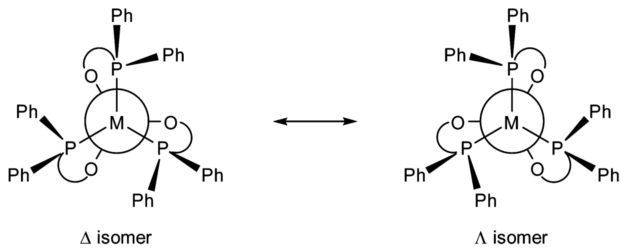

Figure 4. Simplified Newman projection illustrating the helicity of the bimetallic complexes.

In the case of **3−Ni**, two sets of distinct resonances are observed at ambient temperature for the two phenyl groups on the diphenylphosphine substituents. These can be accounted for by the two orientations of the rings either close to perpendicular or along the metal−metal axis, which are visible at elevated temperatures (see the SI). For **3−Pd**, no phenyl resonances are observed at ambient temperature and for **3−Pt** they are strongly broadened.

The coalescence temperatures (T_C) were highest for **3−Ni** at ca. 332 K followed by **3−Pt** at around 314 and 300 K for **3−Pd**. In the case of **3−Pt**, strong broadening and overlapping of unrelated shifts allow only a rough estimation of T_C. This agrees with the other data, making U−Ni the hardest bond and U−Pt the easiest bond to break to interconvert the isomers. Unfortunately, the presence of the paramagnetic U center precludes the calculation of the energy associated with these dynamic processes due to the additional temperature dependence of the chemical shifts.

The broadened $^{31}P\{^1H\}$ resonances appear at 300 K at 93.2 ppm (**3−Ni**), 68.0 ppm (**3−Pd**), and 85.5 ppm (**3−Pt**), with the latter compound showing a $^{31}P-^{195}Pt$ coupling constant of 3742 Hz. These chemical shifts are all higher than the ^{31}P NMR resonances for the "naked equivalent" group 10 metal complexes $M(PPh_3)_3$, M = Ni (21 ppm), Pd (23 ppm), Pt [50 ppm, $^1J(^{31}P-^{195}Pt)$ = 4438 Hz], but the influence from the uranium paramagnet cannot be quantified. In the absence of paramagnetism, a related shift to higher frequency on incorporation of the more electropositive metal has been used as an (unquantified) indication of group 10 metal → metal electron donation.[17,18,36,37,18,19,38] The significantly lower $^{31}P-^{195}Pt$ coupling constant in **3−Pt** compared to $Pt(PPh_3)_3$ can also be taken as an indication of a 4-coordinate platinum(0).[19]

Computational Investigation of 3−Ni and 3−Pd. In order to probe the uranium−TM (transition metal) bonding within **3−M**, we turned to density functional theory (DFT) at the PBE level. Calculated geometric data for **3−Ni** and **3−Pd** are collected in Table 1.[39] As noted above, the agreement between the calculated and experimental structures is excellent, the largest discrepancy being <0.04 Å (for the average Ni−P distances in **3−Ni**).

Natural population analysis (NPA) data are presented in Table 2, from which it can be seen that the two systems have

Table 2. Natural Population Analysis Data for 3−Ni and, in Italics, 3−Pd

	spin density	partial charge	atomic populations
U	2.146	1.079	$5f^{3.12}6d^{1.50}7s^{0.21}7p^{0.01}$
U	*2.137*	*1.198*	*$5f^{3.08}6d^{1.46}7s^{0.19}7p^{0.01}$*
Ni	−0.075	0.091	$3d^{9.39}4s^{0.48}$
Pd	*−0.032*	*0.050*	*$4d^{9.44}5s^{0.47}$*
I	−0.038	−0.277	$5s^{1.88}5p^{5.39}5d^{0.01}$
I	*−0.040*	*−0.298*	*$5s^{1.89}5p^{5.40}5d^{0.01}$*
P (av)	0.000	0.881	
P (av)	*−0.003*	*0.872*	
O (av)	−0.018	−0.700	
O (av)	*−0.018*	*−0.708*	

very similar electronic structures at the NPA level. The spin densities are very much in keeping with a U(IV) system. Partial charges rarely tally well with formal oxidation state, but those calculated here show that the actinide atoms are much more positive than the transition metals and are very close to zero for the latter, in keeping with an M(0) formalism. The population analysis shows that the 10 electrons expected for Ni(0) and Pd(0) are located mainly in the 3d and 4d orbitals, with a small 4s/5s population. The uranium populations show the expected buildup in 5f and 6d, 1.12/*1.08* and 1.50/*1.46* electrons, respectively, above the value expected for U(IV) (data for **3−Pd** in italics). Such buildups are often taken as a measure of the extent to which the 5f and 6d orbitals are involved in covalent bonding with the surrounding ligand framework.[39−41] We are happy to adopt this approach for the early part of the 5f series, and the present data indicate significant involvement of both f- and d-orbitals.

Further insight into **3−Ni** is provided by analysis of the valence natural localized molecular orbitals (NLMOs), the compositions and characters of an α spin selection of which are collected in Table 3 and shown pictorially in Figure 5. NLMOs 110 and 111 are the two U 5f electrons. NLMOs 113 and 114 are strongly iodine-localized (ca. 92%) and pπ in character, while NLMO 128 is I pσ, with a significantly larger (ca. 20%) uranium contribution than the pπ levels. The remaining orbitals (115−118 and 129) are nickel 3d-based. Together with the five β spin equivalents, these NLMOs house the 10 nickel electrons located by the NPA. They separate into $\sigma + 2\pi + 2\delta$ with respect to the U−Ni axis, with differing contributions from the actinide. The δ orbitals (115 and 116) have essentially no uranium contribution, while the π orbitals (117 and 118), also strongly nickel-localized, have slightly larger uranium contributions (similar to those of the iodine pπ-localized orbitals). Finally, NLMO 129 is nickel dσ, with ca. 10% uranium character. The uranium contributions to the iodine-based NLMOs are more 6d-based than 5f, while the reverse is true for the nickel-localized orbitals.

In order to probe further the nature of the U−Ni and U−Pd bonds, we turned to the quantum theory of atoms-in-molecules (QTAIM) approach, which we have used extensively to study the electronic structure of 5f molecules.[26,41−43] Bond critical point (BCP) data are collected in Table 4, together with five different measures of U−TM bond order. The BCP electron and energy densities and the electron density Laplacian (ρ, H, and $\nabla^2\rho$) are very similar for the two target systems and very

DOI: 10.1021/jacs.5b10698
J. Am. Chem. Soc. XXXX, XXX, XXX−XXX

Table 3. Compositions (%) and Principal Characters of Selected α Spin Valence NLMOs of 3−Ni and, in Italics, 3−Pd

NLMO	composition	character
110	99.18 U (99.56 f)	U f
	99.30 U (99.57 f)	
111	94.81 U (2.05 s, 97.24 f); all others <0.78	U f
	97.24 U (1.49 s, 97.74 f)	
113	92.23 I (99.96 p); 6.62 U (59.44 d, 40.29 f)	I pπ
	92.47 I (99.95 p); 6.30 U (59.33 d, 40.48 f)	
114	91.80 I (99.95 p); 8.02 U (54.62 d, 45.20 f)	I pπ
	90.32 I (99.70 p); 9.05 U (50.96 d, 48.62 f)	
115	95.97 Ni (99.98 d); all others <0.95	Ni/*Pd* dδ
	96.17 Pd (99.99 d); all others <0.78	
116	95.97 Ni (99.98 d); all others <0.95	Ni/*Pd* dδ
	96.17 Pd (99.99 d); all others <0.78	
117	92.29 Ni (99.99 d); 5.34 U (40.82 d, 58.49 f)	Ni/*Pd* dπ
	93.55 Pd (99.94 d); 3.61 U (1.56 s, 46.24 d, 52.06 f)	
118	90.60 Ni (99.99 d); 7.13 U (31.02 d, 68.82 f)	Ni/*Pd* dπ
	92.57 Pd (99.96 d); 4.73 U (40.52 d, 59.16 f)	
128	78.17 I (24.36 s, 75.39 p); 20.91 U (18.95 s, 54.48 d, 26.18 f)	I pσ
	79.60 I (24.65 s, 75.09 p); 19.66 U (16.36 s, 56.56 d, 26.61 f)	
129	88.75 Ni (1.21 s, 98.61 d); 10.40 U (3.55 s, 24.54 d, 70.91 f)	Ni/*Pd* dσ
	91.86 Pd (1.41 s, 98.47 d); 6.81 U (5.13 s, 29.41 d, 64.29 f)	

much in keeping with the extensive previous QTAIM studies of metal−metal bonds, in both bulk metals and polynuclear complexes.[44−57] These have suggested that metal−metal bonding should not be pigeon-holed as either closed-shell or shared-shell, but that "metallic" bonding has a topological behavior of its own, possessing neither ionic nor covalent features; metal−metal bonds are identified by relatively low electron density at the BCP and positive $\nabla^2\rho$ (normally associated with closed shell or ionic bonding) and negative H (usually typical of shared shell or covalent bonding).

The BCP ellipticity ε is a measure of the cylindrical symmetry of a bond. Values close to zero are associated with either single or triple bonds, while significant deviations from zero (up to ca. 0.45) are typical of double bond character.[58] For both **3−Ni** and **3−Pd**, ε is very close to zero. The highly nickel localized nature of NLMOs 115−118 and 129 of **3−Ni** strongly suggests that these ellipticities are not indicative of the higher, i.e., triple bond order, and this is supported by the QTAIM delocalization indices δ(U,TM), which are measures of bond order and which are below 1 for both **3−Ni** and **3−Pd**. Table 4 also provides four further U−TM bond order metrics. All of these agree that the U−Ni bond order is less than 1 and that that of U−Pd is smaller than for the 3d analogue. The lower bond orders found for the Pd system are in keeping with the composition of the NLMOs (Table 3). Specifically, the TM-based dσ and dπ orbitals are even more localized on the transition metal in **3−Pd** than in **3−Ni**, leading to reduced U−TM covalency. Although metal−metal bonding interactions typically increase down a transition-metal group,[59] the present NLMO data are consistent with the electronegativities of Ni, Pd, and U, 1.91, 2.20, and 1.38, respectively, on the Pauling scale.[60] The more electronegative 4d element has a more polar interaction with the actinide than does Ni, leading to reduced bond order.

To the best of our knowledge, there are no comparable computational analyses of the bond order in zero oxidation state group 10 complexes containing a homobimetallic metal−metal bond, so we carried out our own calculations on a previously reported low oxidation state system with an unconstrained Ni−Ni (or Pd−Pd) bond, $[(\eta^5\text{-Cp})\text{M}(\text{PEt}_3)]_2$.[61] Unfortunately, while geometry optimization of the 3d system proceeded smoothly, that for the Pd dimer did not, collapsing to a nonsensical solution. Thus, comparative M−M bond data are not available.

In summary, we conclude that the U−Ni and U−Pd interactions have topological features typical of metal−metal bonds. Analysis of the localized orbital structure locates MOs of σ and π symmetry between the actinide and the transition metals, but these are heavily polarized toward the latter, resulting in small orders. **3−Pd** features consistently smaller bond orders than **3−Ni**, in agreement with greater TM σ and π NLMO localization.

In order to probe the extent to which the U−TM interaction is a function of the geometric constraints placed on the metal atoms by the bidentate ligand framework, we have optimized the geometries of the model compounds **3−Ni(m)** and **3−Pd(m)** $[(\text{PH}_3)_3\text{MU}(\text{OH})_3\text{I}$ (M = Ni, Pd)], i.e., with the chelate bridge broken, to ascertain whether L really does flex/twist sufficiently to enable the "ideal" M−M separation. The U−I distances are very similar to those calculated for **3−Ni** and **3−Pd**, 2.993 and 2.995 Å, respectively. By contrast, there is a significant lengthening of the U−TM distances, to 2.784 and 2.932 Å, respectively, for **3−Ni(m)** and **3−Pd(m)**, an increase of ca. 0.25 Å vs **3−Ni** and **3−Pd**. This lengthening is reflected in the QTAIM and bond order metrics for the U−TM interaction, collected in Table 4, which are all smaller (in an absolute sense) than in **3−Ni** and **3−Pd**. As with the full molecules, all of the bond orders are smaller in the model Pd system than the Ni one.

The data on these model compounds therefore indicate that the very short uranium−TM bonds observed in **3−Ni** and **3−Pd** are partly a function of the ligand framework. In the absence of constraining ligands, the 5f−nd bonds lengthen, though uranium−TM interactions are clearly still present. The bond orders in the unchelated compounds are, in general, a little more than half of those calculated for **3−Ni** and **3−Pd**.

Derivatization of the Bimetallic Compounds. In addition to the variation of the d-metal center, we investigated

DOI: 10.1021/jacs.5b10698
J. Am. Chem. Soc. XXXX, XXX, XXX−XXX

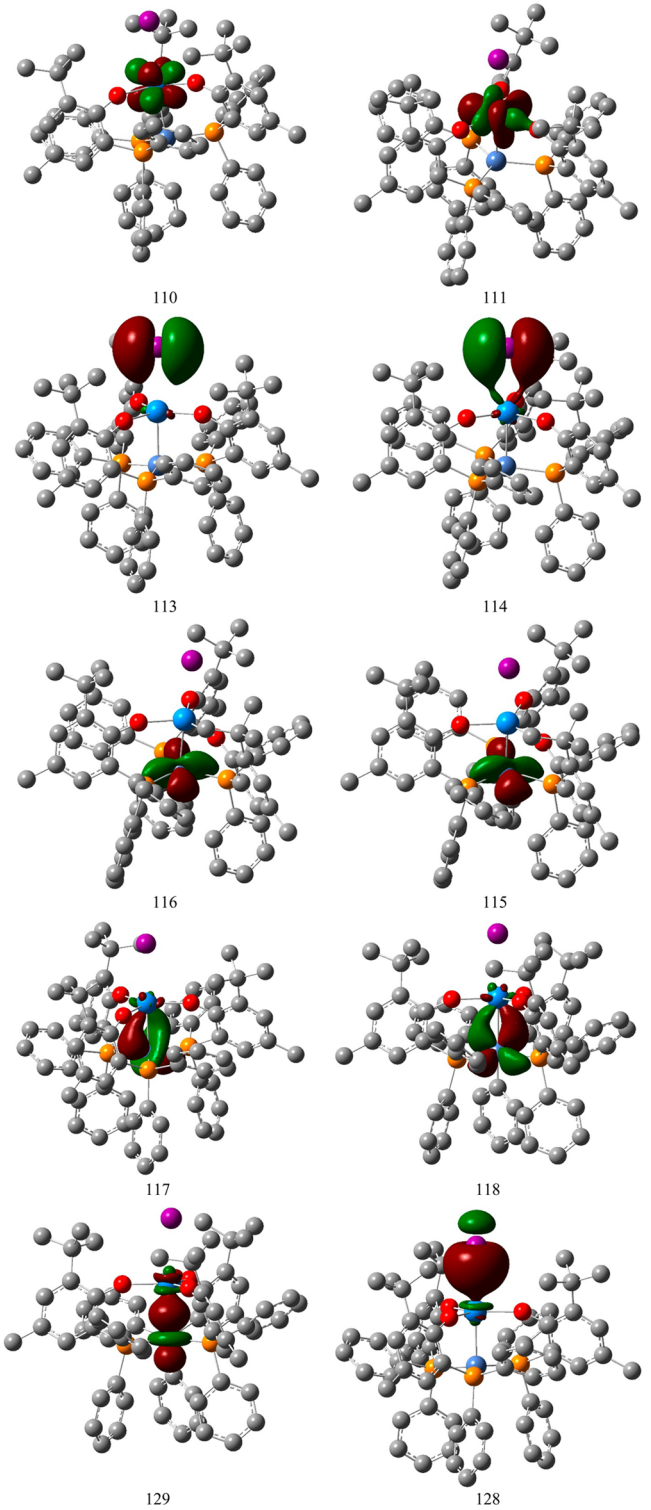

Figure 5. Selected valence NLMOs of **3−Ni**. Isosurface value = 0.04. Atom colors: iodine = purple, uranium = lighter blue, oxygen = red, nickel = darker blue, phosphorus = yellow, and carbon = gray. Hydrogen atoms are omitted for clarity.

the effect on the metal−metal bond of exchanging the iodide for other ligands, focusing on the smaller Ni because of its stronger U−Ni bond. For this purpose it seemed reasonable to substitute the large, polarizable iodide for the more electronegative and strongly bonding fluoride. In order to differentiate between electronic and steric effects, we also included a

Table 4. QTAIM U−TM BCP Parameters and Delocalization Indices and Bond Orders for 3−Ni and 3−Pd and Model Compounds 3−Ni(m) and 3−Pd(m) [$(PH_3)_3MU(OH)_3I$ (M = Ni, Pd)][a]

	3−Ni	3−Pd	3−Ni(m)	3−Pd(m)
ρ	0.068	0.065	0.043	0.041
$\nabla^2\rho$	0.144	0.128	0.064	0.078
H	−0.019	−0.018	−0.010	−0.008
ε	0.024	0.028	0.019	0.012
δ(U,TM)	0.955	0.777	0.633	0.514
Wiberg bond order	0.720	0.625	0.457	0.403
atom−atom net linear NLMO/NPA bond order	0.813	0.685	0.446	0.363
Mayer bond order	0.831	0.598	0.716	0.489
Gopinathan−Jug bond order	0.911	0.640	0.595	0.411

[a] ρ, H, and $\nabla^2\rho$ are in atomic units.

sterically demanding and hard O-donor ligand trimethylsiloxide ($OSiMe_3$). Treatment of **3−Ni** with sodium trimethylsiloxide yields the corresponding uranium(IV) siloxide compound **4** (Scheme 3) and sodium iodide. The reaction of **3−Ni** with

Scheme 3. Preparation of Bimetallic Trimethylsiloxide (4) and Fluoride Derivatives (5)

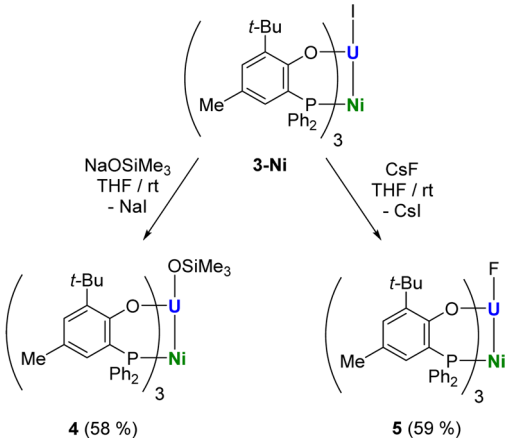

cesium fluoride results in the elimination of cesium iodide to give the $F-U^{IV}-Ni^0$ complex **5** (Scheme 3). Reaction monitoring via ^1H and ^{31}P NMR spectroscopy shows quantitative formation of **4** and **5**, respectively, within 24 h. Attempts to use silver fluoride instead of cesium fluoride resulted in decomposition of the bimetallic species and release of an oxidized nickel(II) complex $Ni^{II}(OAr^P\text{-}\kappa^2O,P)_2$ (**6**), which was characterized crystallographically (see the SI). Adaptation of a published preparation allowed **6** to be prepared independently by reaction of 2 equiv of $HOAr^P$ with 1 equiv of $Ni(cod)_2$ in toluene (see the SI).[62] Reactions of **3−Ni** aimed at the formation of a cationic compound using silver tetraphenylborate or potassium tetraphenylborate gave **6** or no conversion, respectively (see the SI). A bis(trimethylsilyl)-amido derivative of **3−Ni** was also targeted, but the reaction between **3−Ni** and potassium bis(trimethylsilyl)amide did not show any conversion (see the SI).

Dark red crystals of **4** suitable for X-ray crystallography were grown from a benzene/hexane solution at ambient temperature. Single crystals of **5** were obtained from a benzene-layered THF solution. The two bimetallic complexes feature U−Ni bond distances of 2.556(1) Å (**4**) and 2.520(1) Å (**5**) (Figures

DOI: 10.1021/jacs.5b10698
J. Am. Chem. Soc. XXXX, XXX, XXX−XXX

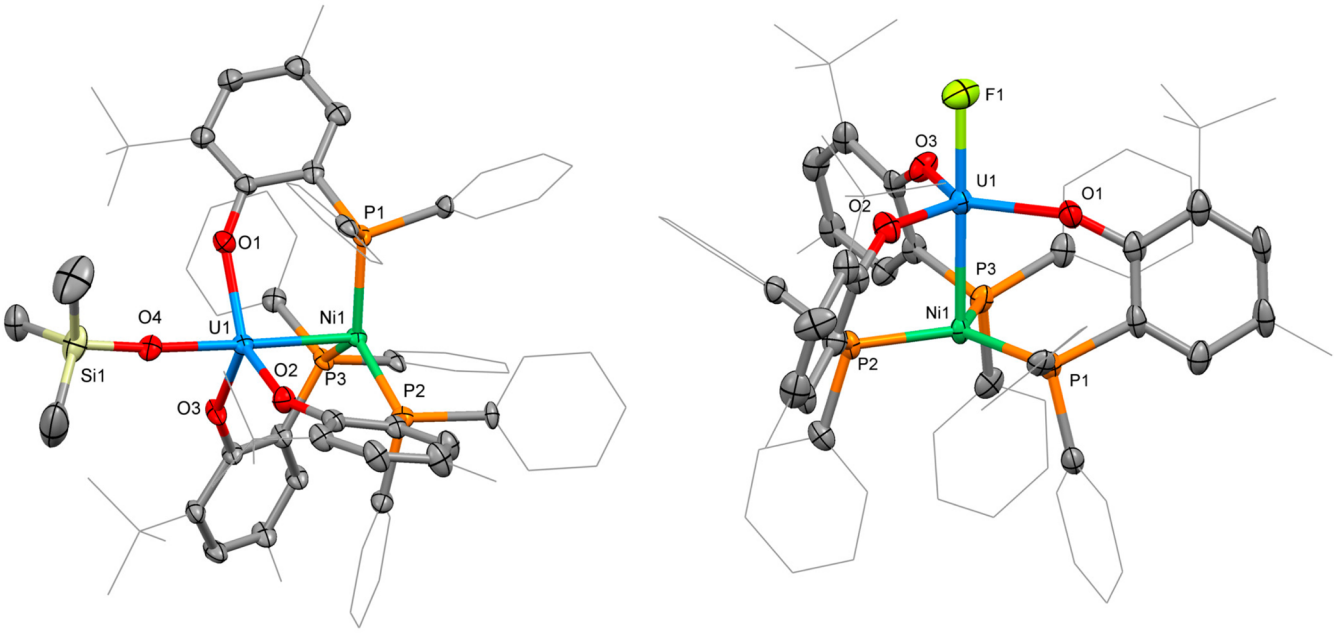

Figure 6. Thermal ellipsoid plots for **4** and **5**. Solvent molecules and hydrogen atoms are omitted, and selected carbon atoms are depicted as a wireframe, for clarity. Thermal ellipsoids drawn at 50% probability. Selected bond distances (Å) and angles (deg) for **4**: U1−Ni1, 2.556(1); U1−O1, 2.210(6); U1−O2, 2.188(6); U1−O3, 2.160(6); U1−O4, 2.093(6); Ni1−P1, 2.208(2); Ni1−P2, 2.213(3); Ni1−P3, 2.221(2); O4−U1−Ni1, 178.6(2); U1−Ni1−P1, 87.85(7); U1−Ni1−P2, 97.84(7); U1−Ni1−P3, 94.95(7); O1−U1−Ni1−P1, 37.4(2); O2−U1−Ni1−P2, 18.4(2); O3−U1−Ni1−P3, 28.1(2). For **5**: U1−Ni1, 2.520(1); U1−F1, 2.091(5); U1−O1, 2.159(8); U1−O2, 2.174(6); U1−O3, 2.199(5); Ni1−P1, 2.225(3); Ni1−P2, 2.215(3); Ni1−P3, 2.212(2); F1−U1−Ni1, 178.8(2); U1−Ni1−P1, 96.16(7); U1−Ni1−P2, 91.56(7); U1−Ni1−P3, 91.82(7); O1−U1−Ni1−P1, 22.2(2); O2−U1−Ni1−P2, 30.1(2); O3−U1−Ni1−P3, 29.1(2).

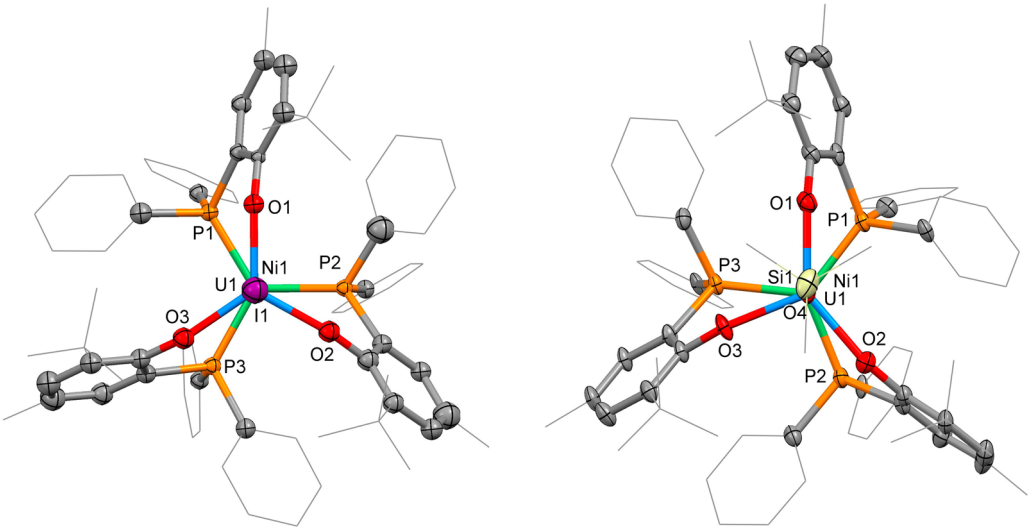

Figure 7. Thermal ellipsoid plot for **3−Ni** (left) and **4** (right) viewed along the U−Ni bond axes. Solvent molecules and hydrogen atoms are omitted and selected carbon atoms are depicted as a wireframe for clarity. Thermal ellipsoids are drawn at 50% probability.

6 and 7), respectively. For **4**, this is slightly longer than in **3−Ni**, likely a result of the increased spatial demand of the $OSiMe_3$ substituent compared with the iodide and thus a greater steric clash with the *tert*-butyl groups of the aryl oxide ligands. However, the exchange of iodide for the smaller, more electronegative fluoride in **5** is accompanied by a decrease of the intermetallic bond distance. While this could be associated with a reorganization of the OAr^P ligand set, it could also be attributed to the inverse trans influence. The siloxide U−O bond distance of 2.093(6) Å in **4** is significantly shorter than the U−O_{Ar} bonds but within the range of previously reported values for uranium(IV) trimethylsiloxides.[63−68] The U−F distance of 2.091(5) Å in **5** is within the range of other nonbridging uranium(IV) fluoride compounds. The Ni−P bonds in **4**, 2.208(1)−2.221(2) Å, and **5**, 2.212(2)−2.225(3) Å, are slightly shorter than in the parent compound, indicating increased back-bonding via the σ^*(Ni−P) orbitals.[69] In the solid state, both the U1−O4−Si1 [174.9(4)°] and Ni1−U1−O4 [178.6(2)°] angles in **4** are nearly linear. The F−U−Ni angle in **5** is 178.8(2)°, similar to that of its congener. The U−F bond dissociation energy is measured to be around 50% stronger than the other U−halide bonds in UX_4, and the U−Ni

DOI: 10.1021/jacs.5b10698
J. Am. Chem. Soc. XXXX, XXX, XXX−XXX

bond length decreases in the order SiO−U−Ni > I−U−Ni > F−U−Ni (i.e., **4** > **3−Ni** > **5**). The ITI would predict a stronger than usual U−O bond in the linearly bound siloxide **4**. If the MM strength order predicted by electrochemistry (vide infra) (SiO−U−Ni > F−U−Ni > I−U−Ni, i.e., **4** > **5** > **3−Ni**) directly correlated with M−M bond length, then the solid-state and solution methods would agree on the halide ordering, perhaps indicating the strongest ITI in the fluoride complex **5**.[70] However, the steric congestion around the U−siloxide evidenced by the solid-state structure and the NMR spectra of **4** suggests that in this instance there is insufficient space for an (ITI-facilitated) closer approach of the O and Ni atoms to U.

The aryloxide U−O bonds in both **4** and **5** are longer than they are in **3−Ni** [2.160(6) to 2.210(6) Å in **4** and 2.159(8) to 2.199(5) Å in **5**], a feature which could be attributed to the preferential shortening of the trans X−U−Ni unit, even for the sterically demanding $OSiMe_3$ group. The top-view of the solid-state structures of the U−Ni iodide and siloxide (**3−Ni** and **4**, respectively) are also shown in Figure 7 to highlight the C_3-propeller shape and similarity of the overall structures.

According to NMR spectroscopy, both **4** and **5** differ significantly in solution from the parent compound **3−Ni**. The ^{1}H NMR resonances for the aryl oxide ligands are in the range from −15.28 to 19.44 ppm for **4** and from −11.70 to 19.04 ppm for **5**, with a more strongly pronounced paramagnetic influence on the ligand sphere compared with **3−Ni**. The proton chemical shift of the trimethylsiloxide group of **4** is 48.67 ppm. Further, the ^{31}P resonances are strongly shifted to high frequencies, 469.4 ppm (**4**) and 474.5 ppm (**5**) (compared with 92.3 ppm for **3−Ni**). Having studied the NLMOs of the complexes involved and not found any significant differences, we attribute the large chemical shift difference to two factors. First, the extensive electronic differences of I vs F/TMSO. Second, the slightly shorter Ni−P bonds in **4** than **5** that indicate stronger Ni−P backbonding. Both of these would combine to enhance the through-bond paramagnetic influence from the f^2-uranium center. Resonances for the heteronuclei ^{19}F and ^{29}Si could not be observed within the spectral range from −740 to 620 and −1050 to 870 ppm, respectively. VT NMR experiments of **4** and **5** show that both have rigid structures in solution as high as 100 °C. This represents a significantly higher energy barrier to the interconversion of Δ and Λ isomers compared with **3**, supporting the ITI-induced stronger U−M bond being formed when the more electronegative X-ligands are uranium-bound. The replacement of the iodide changes the magnetic moment values from 1.9 μ_B (**3−Ni**) to 2.8 μ_B (**4**) and 2.1 μ_B (**5**), respectively. Similarity of magnetic moment throughout series of U(IV) aryl oxide and amide complexes with different halides has been reported.[71−73] The value of the trimethylsiloxide derivative **4** is similar to that of other R_3SiO-ligated uranium complexes, $U(OSiBu_3^t)_4$ (2.83 μ_B) and $U(OSiMe_3)_2I_2(bipy)_2$ (bipy = 2,2′-bipyridine) (2.7 μ_B).[65,74] To account for these increases, and the strongly paramagnetically shifted ^{31}P chemical shifts for **4** and **5**, we compared the composition of the two f-based NLMOs for the iodide (**3−Ni**) and fluoride (**5**) to look for different U 5f contributions that would lead to larger paramagnetic shifts for the Ni-bound atoms. For the iodide, they are 99.18% U (99.56% 5f) and 94.81% U (97.24 5f, 2.05 s, 1.75% total contribution from P) (see also Table S4 of the SI for a comparison of the predominantly Ni d-σ and π NLMOs). For the fluoride they are 99.22% U (99.68% 5f) and 92.54% U (97.58 5f, 1.63 s, 2.48% total contribution from P). While these data indicate a marginally greater through-bond mixing of unpaired 5f electron with the phosphorus, there is really very little difference between the two systems.

The electronic absorption spectra of toluene solutions of the compounds **2−5** were recorded to locate potential metal−metal charge transfer bands (see the SI). UV−vis spectra of monometallic **2** show several weak U(IV) f−f transitions[75] up to ca. 700 nm and more intense $\pi-\pi^*$ charge-transfer processes below 500 nm.[76,77] The second metalation to form **3−Ni**, **3−Pd**, and **3−Pt** causes a bathochromic shift of the predominately ligand-based absorption at short wavelengths. In the visible region, the nickel derivative **3−Ni** differs significantly from **3−Pd** and **3−Pt**, with an absorption at 511 nm (ε 598 M^{-1} cm^{-1}) that is much stronger than that in **4** and **5**, with weaker absorptions at 527 nm (ε 103 M^{-1} cm^{-1}) and 533 nm (ε 90 M^{-1} cm^{-1}), respectively. In the NIR region the monometallic complex **2** shows several absorption bands in the 850−2060 nm region (ε 18−45 M^{-1} cm^{-1}). The NIR spectra of **3−Ni**, **3−Pd**, and **3−Pt** are similar to each other but feature fewer absorption bands. As such, an unambiguous assignment of absorptions in this region to a metal−metal charge transfer appears to be not possible.

ELECTROCHEMISTRY

The electronic structures of complexes **2−5** were investigated using a range of voltammetric techniques (Figure 8 and the SI).

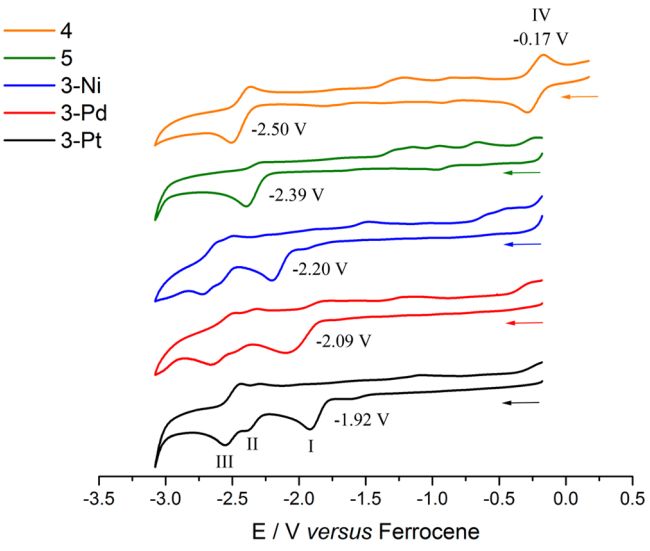

Figure 8. Cyclic voltammograms for **3−Pt**, **3−Pd**, **3−Ni**, **4**, and **5**. All measured in THF using 0.1 M $[^nBu_4N][BPh_4]$ as the supporting electrolyte, at a scan rate of 100 mV s^{-1}. The currents are normalized against the peak height of reduction process I for **3−Pt**.

In the electrochemical window provided by THF/$[^nBu_4N][BPh_4]$, a single reduction process was observed for **2** during the cyclic voltammetry (CV) experiment, at E_p^c −2.87 V versus Fc^+/Fc, assigned to the U(IV)/U(III) couple and it is irreversible. The U(IV)/U(III) redox couple is sensitive to the ligand environment and has been reported in the range from −1.83 to −2.78 V for metallocene and acetylacetonate (acac) complexes.[78−80]

Incorporation of the group 10 transition metal alters the electrochemistry significantly. The CVs of **3−Ni**, **3−Pd**, and **3−Pt** are qualitatively very similar, having three reduction processes each, suggesting a common electronic structure. The

DOI: 10.1021/jacs.5b10698
J. Am. Chem. Soc. XXXX, XXX, XXX−XXX

electrochemical behavior of **3−Pt** will be described as a representative example. The first reduction (denoted I) at E_p^c −1.92 V is irreversible; two further quasi-reversible reduction processes are observed as overlapping cathodic waves at E_p^c −2.39 and −2.55 V, denoted II and III, respectively. Determination of the peak areas in the CV of **3−Pt** reveals that the charge passed during reduction I is equal to that passed during II and III combined, indicating that process I is a two-electron reduction, whereas II and III are single-electron reduction processes.

The electrochemical experiments with **3−Ni** and **3−Pd** generated identical conclusions, and in the series **3**, the reduction potentials for all three processes are cathodically shifted when the transition metal is changed from Pt to Pd to Ni. The Kohn−Sham α spin LUMOs of both **3−Ni** and **3−Pd** are primarily U−M antibonding, so we ascribe reduction I to the filling of this orbital and conclude that the cathodic shift of the reduction process moving up the group 10 metals is due to a strengthening of the metal−metal bond.[81] This agrees with the computational results that showed higher bond order for **3−Ni** compared to **3−Pd** and also correlates with the shorter M−M′ distance determined crystallographically.

The CV of **5**, the fluoride analogue of **3−Ni**, shows only an irreversible reduction at E_p^c −2.39 V, but square-wave voltammetry (SWV) reveals a second process at the edge of the electrochemical window, E_p^c −2.81 V. This implies that **5** displays similar electrochemical behavior to the iodo complexes, albeit at more negative potentials; i.e., replacing the iodide with a fluoride strengthens the metal−metal bond trans to it.

The replacement of iodide with siloxide to make **4** cathodically shifts the reduction I further still, to E_p^c −2.50 V; no other reduction processes are observed by CV or SWV. This reduction is now quasi-reversible and suggests that the reduced species is stabilized to a certain degree. A reversible oxidation process is also observed at $E_{1/2}$ −0.20 V, denoted IV. The area of the anodic CV wave for IV is approximately equal to the area of the cathodic wave for reduction I, and both processes therefore involve two electrons. It is not known whether this oxidation IV is unique to **4**; it may be that this oxidation is possible for all but lies outside of the electrochemical window.

Thus, we infer from the electrochemical data that the metal−metal bond strength increases in the series **3−Pt** < **3−Pd** < **3−Ni** < **5** < **4**.

CONCLUSIONS

The use of a relatively rigid heterobidentate phosphinoaryl oxide ligand that forms strong U−O bonds and weak, labile U−P bonds in the new complex $IU^{IV}(OAr^P\text{-}\kappa^2O,P)_3$ has allowed the systematic incorporation of Ni(0), Pd(0), or Pt(0) via phosphine coordination, and the replacement of the iodide anion with Me_3SiO^- or F^-, to form a set of five heterobimetallic U−M complexes $XU^{IV}(\mu\text{-}OAr^P\text{-}1\kappa^1O,2\kappa^1P)_3M^0$ (X = I, $OSiMe_3$, F; M = Ni, Pd, Pt), all of which have shorter An−TM bonds than any previously reported example. The synthesis of a complete set of adducts from a single group for the first time and the solution and solid-state structural characterization of the complexes have enabled a thorough study of the uranium−metal bond. The U−I bond length in the starting material **2** becomes significantly shorter upon formation of the U−M complexes **3**, but the coordination number changes from 7 to 5 (replacing three phosphines with one metal center), so inferences of the inverse trans influence (ITI) cannot be made here. Upon introduction of the group 10 metal centers, the magnetic moment decreases from 2.4 μ_B to around 1.9 μ_B in **3**, respectively, an opposite change in moment to that reported upon secondary metalation of U complexes by Co^I as a donor.[10]

Although the changes in magnetic moment and UV−vis−NIR spectra cannot yet be interpreted in terms of bonding trends in the series, the combination of experimental electrochemistry and computation is particularly informative. A cathodic shift of the first reduction process observed upon moving from U−Pt up to U−Ni indicates a strengthening of the metal−metal bond in the order **3−Ni** > **3−Pd** > **3−Pt**. This correlates with the shortening of the internuclear distance determined crystallographically. Natural population analysis and natural localized molecular orbital compositions indicate that U employs both its 5f and 6d orbitals in covalent bonding to a significant extent, and this agrees with experimental data that the oxidation states of the metals are best described as U(IV) and zero for the group 10 atoms. Quantum theory of atoms-in-molecules analysis yields bond critical point properties in keeping with many previous studies of transition-metal−metal bonds in both bulk metals and polynuclear clusters (relatively low electron density, positive $\nabla^2\rho$, and negative H). Replacing the uranium-bound iodide trans to the nickel center with the more electronegative fluoride and siloxide also results in NMR spectroscopic and electrochemical responses consistent with a strengthening of the U−Ni bond and with the existence of an ITI. If an ITI is influencing the M−M′ bond strength, then this is also borne out by the crystallographic data for **3** and **5**, which show a shorter U−Ni bond in the F−U−Ni (**5**) than in I−U−Ni (**3**) complexes. Despite the short U−M distances, the bond orders are calculated by five different approaches to be small; less than 1 in all cases. All bond order metrics are smaller for U−Pd than U−Ni, in agreement with the electrochemical and QTAIM bond critical point data and with population analysis of the U−TM σ and π NLMOs which, while heavily localized on the TM in both cases, are even more so for the 4d system than the 3d, in keeping with the larger electronegativity difference between U and Pd vs U and Ni. Calculations on a monodentate analogue of **3** show that in the absence of the constraining ligand geometry there is clearly still a U−TM interaction, but it is enhanced by about 0.25 Å in the constraining ligand framework.

Thus, by combining the spectroscopic, computational, electrochemical, and structural studies, the U−M bond strength can be placed in increasing order: **3−Pt** < **3−Pd** < **3−Ni** < **5** < **4**, i.e., I−U−Pt < I−U−Pd < I−U−Ni < F−U−Ni < SiO−U−Ni.

EXPERIMENTAL SECTION

General Details. All manipulations were carried out under a dry, oxygen-free atmosphere of nitrogen using standard Schlenk and glovebox technique. Benzene was distilled from potassium and stored over 4 Å molecular sieves. Hexane, THF, and toluene were degassed and purified by passage through activated 4 Å molecular sieves or activated alumina towers and stored over 4 Å molecular sieves. Deuterated solvents, benzene-d_6 and toluene-d_8, were boiled over potassium, vacuum-transferred, and freeze−pump−thaw degassed prior to use. ^{1}H, ^{13}C, ^{19}F, ^{29}Si, and ^{31}P NMR spectra were recorded on Bruker AVA400, AVA500, or PRO500 spectrometers at 300 K. Variable-temperature NMR spectra were recorded on a Bruker AVA400 spectrometer between 300 and 370 K. Chemical shifts are reported in parts per million, δ, referenced to residual proton resonances, and calibrated against external TMS. Magnetic moment

DOI: 10.1021/jacs.5b10698
J. Am. Chem. Soc. XXXX, XXX, XXX−XXX

values were determined by Evans' method using a sealed benzene-d_6 capillary as reference.[82−85] UV−vis−NIR spectra were recorded on a JASCO V-670 spectrophotometer using a sealed quartz cuvette with 0.02−5 mM toluene solutions. Artifacts at 1650−1750 nm relate to solvent absorption. Electrochemical measurements were made on 1−10 mM of the analyte in 12 cm^3 THF, 0.1 M [^{n}Bu$_4$N][BPh$_4$], in a N_2-filled glovebox using an Autolab ECO Chemie PGSTAT potentiostat, glassy-carbon disk (d = 3 mm) working electrode, Pt-gauze counter electrode, Ag-wire quasi-reference electrode, and ferrocenium/ferrocene (Fc^+/Fc = 0 V) standard.[86] Scan details are in the SI, and data were processed using GPES Manager 4.9. Elemental analyses were carried out at London Metropolitan University, London, UK, and Pascher Labor, Remagen, Germany. $UI_4(dioxane)_{1.5}$,[87] HOC_6H_2-6-Bu^t-4-Me-2-PPh_2,[32] and $AgBPh_4$[88] were prepared according to published procedures. All other reagents were from commercial sources and used as received.

KOC$_6$H$_2$-6-Bu^t-4-Me-2-PPh$_2$ (KL, 1). A Schlenk flask was charged with 6-*tert*-butyl-4-methyl-2-(diphenylphosphino)phenol (5.92 g, 17.0 mmol, 1 equiv), potassium hydride (682 mg, 17.0 mmol, 1 equiv), and a stir bar and cooled in an ice bath. THF (40 mL) was added under vigorous stirring, and the mixture was allowed to warm to 20 °C after 30 min, and no further H_2 evolution was observable. After storage at 5 °C for 18 h, the colorless solids were isolated via filtration, washed with hexane (3 × 10 mL), and dried in vacuo to give **1** as a colorless powder (5.33 g, 81%). ^{1}H NMR (THF-d_8): 1.40 (s, 9H, *t*Bu), 1.93 (s, 3H, Me), 5.99 (m, 1H, ArH), 6.79 (d, $^4J_{H,H}$ 2.4 Hz), 7.20−7.26 (m, 6H, Ph), 7.30−7.34 (m, 4H, Ph). ^{13}C NMR (THF-d_8): 21.4, 30.4, 35.4 (d, $^4J_{C,P}$ 2.3 Hz), 116.8 (d, $^3J_{C,P}$ 3.1 Hz), 122.4 (d, $^1J_{C,P}$ 13.8 Hz), 128.6 (d, $^2J_{C,P}$ 6.5 Hz), 128.6, 135.0 (d, $^3J_{C,P}$ 18.8 Hz), 136.2 (d, $^3J_{C,P}$ 1.5 Hz), 142.2 (d, $^1J_{C,P}$ 11.5 Hz), 171.1 (d, $^1J_{C,P}$ 17.2 Hz). ^{31}P{^{1}H} NMR (THF-d_8): −15.0. Anal. Calcd for $C_{23}H_{24}KOP$: C 71.47. H 6.26. Found: C 71.56, H 6.31.

IU(μ-OC$_6$H$_2$-6-Bu^t-4-Me-2-PPh$_2$-κ^2*O*,*P*)$_3$ (IUL$_3$, 2). A Schlenk flask was charged with $UI_4(Et_2O)_2$ (2.68 g, 3.00 mmol), a stir bar, and THF (20 mL). Under vigorous stirring a THF solution of **1** (3.48 g, 9.00 mmol, 3.00 equiv, 30 mL) was added via syringe. The green mixture was stirred at room temperature for 16 h, followed by evaporation of volatiles under reduced pressure. The green residue was extracted four times with warm toluene. The green extract was concentrated to 40 mL and stored at −30 °C, giving 3.28 g (78%) of **2** as a bright green powder. ^{1}H NMR (toluene-d_8): 4.96 (v br). ^{1}H NMR (toluene-d_8, 370 K): 1.83 (br), 4.88 (br), 5.12, 5.30 (br), 6.54 (v br), 8.89 (v br), 15.10 (v br). Evans' method (C_6D_6): 2.4 μ_B. UV−vis−NIR [λ in nm (ε in M^{-1} cm^{-1})]: 300 (1.8 × 10^4), 516 (38), 550 (18), 598 (16), 633 (26), 895 (29), 976 (19), 1023 (27), 1069 (31), 1102 (35), 1139 (32), 1175 (27), 1198 (26), 1351 (22), 1406 (27), 1484 (18), 1829 (10), 2055 (45). Anal. Calcd for $C_{69}H_{72}IO_3P_3U$: C 58.89. H 5.16. Found: C 59.03, H 5.06.

IU^{IV}L$_3$Ni^0 (3−Ni). A Schlenk flask equipped with a stirring bar was charged with **2** (422 mg, 0.300 mmol) and bis(1,8-cyclooctadiene)-nickel (28 mg, 0.30 mmol, 1.0 equiv). The reagents were dissolved in toluene (20 mL) to give a red solution and stirred at ambient temperature for 18 h, during which time the mixture turned dark red and deposited a metal mirror. After removal of volatiles under reduced pressure, the dark red residue was extracted with warm toluene (3 × 5 mL). The combined extracts were concentrated to ca. 10 mL and stored at −30 °C for 1 d. Dark red crystals of **3−Ni** were isolated, washed with hexane, and dried in vacuo. Yield: 316 mg (72%). ^{1}H NMR (toluene-d_8): 3.51 (s, 9H, Ar*Me*), 4.05 (s, 6H, PPh*H*), 4.66 (s, 6H, PPh*H*), 4.97 (s, 6H, PPh*H*), 5.74 (s, 6H, PPh*H*), 5.93 (s, 30H, *t*Bu/PPh*H*$_p$), 6.29 (s, 3H, PPh*H*$_p$), 6.35 (s, 3H, Ar*H*), 11.65 (s, 3H, Ar*H*). ^{1}H NMR (toluene-d_8, 370 K): 3.30 (s, 9H, Ar*Me*), 4.61 (s, 12H, PPh*H*), 5.07 (s, 27H, *t*Bu), 5.57 (s, 6H, PPh*H*), 6.22 (s, 6H, PPh*H*$_p$), 6.32 (s, 3H, Ar*H*), 11.03 (s, 3H, Ar*H*). ^{31}P{^{1}H} NMR (C_6D_6): 92.3. Evans' method (C_6D_6): 1.9 μ_B. UV−vis−NIR [λ in nm (ε in M^{-1} cm^{-1})]: 305 (3.4 × 10^4), 511 (598), 666 (41), 709 (51), 814 (8), 948 (13), 1056 (25), 1120 (36), 1202 (39), 1411 (13), 1547 (15), 1649 (14), 1748 (15), 1754 (15). Anal. Calcd for $C_{69}H_{72}INiO_3P_3U$: C 56.54. H 4.95. Found: C 56.65, H 5.01.

IU^{IV}L$_3$Pd^0 (3−Pd). A Schlenk flask was charged with **2** (141 mg, 0.100 mmol), tetrakis(triphenylphosphine)palladium (116 mg, 0.100 mmol, 1.00 equiv), a stir bar, and toluene (5 mL) and the solution stirred at 80 °C for 3 d. The red mixture was cannula filtered, layered with hexane, and allowed to stand at ambient temperature. Orange crystals of **3−Pd** grew over 5 d and were isolated by decanting, washed with hexane, and dried under vacuum. Yield: 53 mg (35%). ^{1}H NMR (toluene-d_8): 5.32 (s, 9H, Ar*Me*), 7.23 (s, 3H, Ar*H*), 9.89 (s, 27H, tBu), 15.44 (s, 3H, Ar*H*). ^{1}H NMR (toluene-d_8, 370 K): 3.21 (s, 12H, *o*-*H*PhP), 4.63 (s, 9H, Ar*Me*), 5.60 (s, 12H, *m*-*H*PhP), 6.11 (s, 6H, *p*-*H*PhP), 7.11 (s, 3H, Ar*H*), 7.83 (s, 27H, tBu), 13.69 (s, 3H, Ar*H*). ^{31}P{^{1}H} NMR (C_6D_6): 68.4. ^{31}P{^{1}H} NMR (toluene-d_8): 68.0. Evans' method (C_6D_6): 1.8 μ_B. UV−vis−NIR [λ in nm (ε in M^{-1} cm^{-1})]: 300 (3.4 × 10^4), 527 (103), 576 (27), 661 (22), 686 (29), 722 (11), 891 (9), 948 (13), 1060 (19), 1114 (34), 1151 (23), 1175 (19), 1431 (11), 1455 (12), 1540 (16), 1750 (11), 1776 (12), 2045 (12), 2086 (13). Anal. Calcd for $C_{69}H_{72}IO_3P_3PdU$: C 54.75. H 4.79. Found: C 54.82, H 4.88.

IU^{IV}L$_3$Pt^0 (3−Pt). This compound was prepared in an analogous procedure to that of **3−Pd** (see the SI) to give orange crystals in 66% yield.

Me$_3$SiOU^{IV}L$_3$Ni^0 (4). A scintillation vial was charged with **3−Ni** (147 mg, 0.100 mmol), sodium trimethylsilanolate (11 mg, 0.10 mmol, 1.0 equiv), a stir bar, and THF (3 mL). The red mixture was stirred for 16 h at ambient temperature and then evaporation of volatiles under reduced pressure, affording a dark red residue which was suspended in a minimal amount of benzene, centrifuged, and filtered. Dark red crystals of **4** were isolated from the benzene filtrate by hexane vapor diffusion (83 mg, 58%). ^{1}H NMR (toluene-d_8): −15.47 (s, 27H), −7.59 (s, 3H), −7.20 (br s, 3H), −4.74 (t, 3H, *J* 7.5 Hz), −3.95 (s, 9H), 7.65 (s, 3H), 16.82 (t, 3H, *J* 7.5 Hz), 19.47 (br s, 3H), 48.83 (s, 9H). ^{1}H NMR (toluene-d_8, 370 K): −11.57 (s, 27H), −4.23 (s, 3H), −4.13 (br s, 3H), −3.83 (vbr s, 3H), −2.59 (s, 9H), −2.15 (br s, 3H), 7.29 (s, 3H), 14.56 (t, 3H, *J* 7.5 Hz), 16.56 (s, 6H), 30.38 (vbr s, 6H), 37.77 (s, 9H). 469.4. ^{31}P{^{1}H} NMR (toluene-d_8): 476.4. Evans' method (C_6D_6): 2.8 μ_B. UV−vis−NIR [λ in nm (ε in M^{-1} cm^{-1})]: 302 (2.9 × 10^4), 520 (296), 559 (148), 659 (50), 692 (28), 837 (6), 966 (22), 1098 (31), 1150 (38), 1287 (16), 1410 (10), 1578 (20), 1751 (22), 1781 (31), 1885 (48), 2039 (7), 2075 (4). Anal. Calcd for $C_{72}H_{81}O_4P_3SiU$: C 60.55. H 5.72. Found: C 60.43. H 5.81.

FU^{IV}L$_3$Ni^0 (5). A scintillation vial was charged with **3−Ni** (58 mg, 0.040 mmol, 1.0 equiv), cesium(I) fluoride (6 mg, 0.040 mmol, 1.0 equiv), a stir bar, and THF (2 mL). The red solution was stirred for 1 d at ambient temperature. Some colorless solids that formed were removed by filtration. Volatiles were removed under reduced pressure, the red residue was suspended in benzene, and the solution was centrifuged and then filtered. Crystallization by hexane vapor diffusion into the filtrate afforded red crystals (32 mg, 59%) of **5**. ^{1}H NMR (toluene-d_8): −11.88 (s, 27H), −7.35 (s, 3H), −7.25 (s, 4H), −4.74 (s, 3H), −4.25 (s, 9H), 5.73 (br s, 2H), 6.54 (s, 3H), 16.58 (s, 3H), 19.16 (v br s, 6H), 30.00 (v br s, 4H). ^{1}H NMR (toluene-d_8, 370 K): −8.60 (s, 27H), −4.06 (br s, 12H), −2.86 (s, 9H), −2.10 (br s, 2H), 5.10 (s, 3H), 6.36 (s, 2H), 14.37 (s, 3H), 16.31 (br s, 4H), 30.00 (v br s, 4H). ^{31}P{^{1}H} NMR (C_6D_6): 474.5. Evans' method (C_6D_6): 2.1 μ_B. UV−vis−NIR [λ in nm (ε in M^{-1} cm^{-1})]: 303 (2.5 × 10^4), 655 (147), 691 (118), 841 (73), 952 (75), 1042 (64), 1087 (75), 1150 (82), 1202 (48), 1254 (49), 1412 (35), 1447 (29), 1580 (39), 1751 (57), 1777 (77), 1835 (81), 1880 (66), 2035 (15), 2072 (12). Anal. Calcd for $C_{69}H_{72}FO_3P_3U$: C 61.03. H 5.34. Found: C 60.89, H 5.23.

Computational Details. Density functional theory calculations were carried out using the PBE functional, as implemented in Gaussian 09, Rev. C.01 and D.01,[89] and ADF 2014[90−92] quantum chemistry codes. For the Gaussian calculations, the cc-pVDZ basis set was used for all atoms except U, I, and Pd. For these elements, a Stuttgart−Bonn variety relativistic pseudopotential was employed, together with segmented valence basis sets; (14s13p10d8f)/[10s9p5d4f] for U,[93] (16s12p4d1f)/[3s3p2d1f] for I,[94,95] and (8s7p6d2f)/[6s5p3d1f] for Pd.[95,96] The ultrafine integration grid was employed. natural bond orbital calculations were performed using the NBO6 code, interfaced with Gaussian revision D.01.[97] QTAIM analyses were performed using

DOI: 10.1021/jacs.5b10698
J. Am. Chem. Soc. XXXX, XXX, XXX−XXX

the AIMAll program package,[98] with .wfx files generated in Gaussian used as input.

Single-point calculations, at the Gaussian-optimized geometries, were run in the ADF code in order to obtain Mayer[99] and Gopinathan–Jug[100] bond orders. For these calculations, the zeroth-order regular approximation (ZORA) Hamiltonian was used. Slater-type orbital ZORA basis sets of TZP quality were used for U, Ni, Pd, and I, with DZP ZORA basis sets for all other atoms. The frozen core approximation was employed, with U(5d), I(4p), Pd(3d), Ni(2p), P(2p), and 1s for all other atoms, bar H. The default SCF convergence criteria were used, together with an integration grid of 4.5.

■ ASSOCIATED CONTENT

Supporting Information

The Supporting Information is available free of charge on the ACS Publications website at DOI: 10.1021/jacs.5b10698. Crystallographic files were deposited at the Cambridge Crystallographic Data Centre (CCDC): 1430506 (**2**), 1430507 (**3–Ni**), 1430511 (**3–Pd**), 1430512 (**3–Pt**), 1430513 (**4**), 1438934 (**5**), and 1430514 (**6**). Open data files are available at DOI: 10.7488/ds/1351.

> Crystallographic data, additional variable-temperature NMR spectra, additional synthetic data, including other reactivity studies, and solid-state structure details of all complexes (PDF).

■ AUTHOR INFORMATION

Corresponding Authors

*nikolas.kaltsoyannis@manchester.ac.uk
*polly.arnold@ed.ac.uk

Notes

The authors declare no competing financial interest.

■ ACKNOWLEDGMENTS

We thank EaStCHEM, the University of Edinburgh and the Engineering and Physical Sciences Research Council EPSRC (grants EP/H004823/1 and EP/M010554/1). J.A.H. thanks the Austrian Science Fund (FWF) for funding via Erwin Schrödinger Fellowship project J-3467. N.K. thanks University College London for computing resources via the Research Computing "Legion" cluster Legion@UCL and associated services and The University of Manchester for access to its Computational Shared Facility, and he is also grateful for computational resources from the EPSRC's National Service for Computational Chemistry Software, http://www.nsccs.ac.uk. P.L.A. also thanks the Technische Universität München—Institute for Advanced Study, funded by the German Excellence Initiative.

■ REFERENCES

(1) Cooper, B. G.; Napoline, J. W.; Thomas, C. M. *Catal. Rev.: Sci. Eng.* **2012**, *54*, 1–40.
(2) Liddle, S. T.; Mills, D. P. *Dalton Trans.* **2009**, 5592–5605.
(3) Patel, D.; Liddle, S. T. *Rev. Inorg. Chem.* **2012**, *32*, 1–22.
(4) Oelkers, B.; Butovskii, M. V.; Kempe, R. *Chem. - Eur. J.* **2012**, *18*, 13566–13579.
(5) Sternal, R. S.; Marks, T. J. *Organometallics* **1987**, *6*, 2621–2623.
(6) Bucaille, A.; Le Borgne, T.; Ephritikhine, M.; Daran, J.-C. *Organometallics* **2000**, *19*, 4912–4914.
(7) Monreal, M. J.; Khan, S. I.; Kiplinger, J. L.; Diaconescu, P. L. *Chem. Commun.* **2011**, *47*, 9119.
(8) Gardner, B. M.; Patel, D.; Cornish, A. D.; McMaster, J.; Lewis, W.; Blake, A. J.; Liddle, S. T. *Chem. - Eur. J.* **2011**, *17*, 11266–11273.
(9) Patel, D.; Moro, F.; McMaster, J.; Lewis, W.; Blake, A. J.; Liddle, S. T. *Angew. Chem., Int. Ed.* **2011**, *50*, 10388–10392.
(10) Napoline, J. W.; Kraft, S. J.; Matson, E. M.; Fanwick, P. E.; Bart, S. C.; Thomas, C. M. *Inorg. Chem.* **2013**, *52*, 12170–12177.
(11) Ward, A. L.; Lukens, W. W.; Lu, C. C.; Arnold, J. *J. Am. Chem. Soc.* **2014**, *136*, 3647–3654.
(12) Gardner, B. M.; McMaster, J.; Lewis, W.; Liddle, S. T. *Chem. Commun.* **2009**, 2851–2853.
(13) Gardner, B. M.; McMaster, J.; Moro, F.; Lewis, W.; Blake, A. J.; Liddle, S. T. *Chem. - Eur. J.* **2011**, *17*, 6909–6912.
(14) Patel, D.; King, D. M.; Gardner, B. M.; McMaster, J.; Lewis, W.; Blake, A. J.; Liddle, S. T. *Chem. Commun.* **2011**, *47*, 295–297.
(15) Fortier, S.; Walensky, J. R.; Wu, G.; Hayton, T. W. *J. Am. Chem. Soc.* **2011**, *133*, 11732–11743.
(16) Arnold, P. L.; McMaster, J.; Liddle, S. T. *Chem. Commun.* **2009**, 818–820.
(17) Roussel, P.; Scott, P. *J. Am. Chem. Soc.* **1998**, *120*, 1070–1071.
(18) Ritchey, J. M.; Zozulin, A. J.; Wrobleski, D. A.; Ryan, R. R.; Wasserman, H. J.; Moody, D. C.; Paine, R. T. *J. Am. Chem. Soc.* **1985**, *107*, 501–503.
(19) Hay, P. J.; Ryan, R. R.; Salazar, K. V.; Wrobleski, D. A.; Sattelberger, A. P. *J. Am. Chem. Soc.* **1986**, *108*, 313–315.
(20) Nakajima, Y.; Hou, Z. *Organometallics* **2009**, *28*, 6861–6870.
(21) Völcker, F.; Mück, F. M.; Vogiatzis, K. D.; Fink, K.; Roesky, P. W. *Chem. Commun.* **2015**, *51*, 11761–11764.
(22) Van der Sluys, W. G.; Burns, C. J.; Huffman, J. C.; Sattelberger, A. P. *J. Am. Chem. Soc.* **1988**, *110*, 5924–5925.
(23) Van der Sluys, W. G.; Sattelberger, A. P. *Inorg. Chem.* **1989**, *28* (12), 2496–2498.
(24) Avens, L. R.; Barnhart, D. M.; Burns, C. J.; McKee, S. D.; Smith, W. H. *Inorg. Chem.* **1994**, *33*, 4245–4254.
(25) McKee, S. D.; Burns, C. J.; Avens, L. R. *Inorg. Chem.* **1998**, *37*, 4040–4045.
(26) Mansell, S. M.; Kaltsoyannis, N.; Arnold, P. L. *J. Am. Chem. Soc.* **2011**, *133*, 9036–9051.
(27) Arnold, P. L.; Mansell, S. M.; Maron, L.; McKay, D. *Nat. Chem.* **2012**, *4*, 668–674.
(28) O'Grady, E.; Kaltsoyannis, N. *Dalton Trans.* **2002**, 1233–1239.
(29) Kosog, B.; La Pierre, H. S.; Heinemann, F. W.; Liddle, S. T.; Meyer, K. *J. Am. Chem. Soc.* **2012**, *134*, 5284–5289.
(30) Lewis, A. J.; Mullane, K. C.; Nakamaru-Ogiso, E.; Carroll, P. J.; Schelter, E. J. *Inorg. Chem.* **2014**, *53*, 6944–6953.
(31) La Pierre, H. S.; Rosenzweig, M.; Kosog, B.; Hauser, C.; Heinemann, F. W.; Liddle, S. T.; Meyer, K. *Chem. Commun.* **2015**, *51*, 16671–16674.
(32) Klein, H.-F.; Brand, A.; Cordier, G. *Z. Naturforsch., B: J. Chem. Sci.* **1998**, *53*, 307–314.
(33) Edwards, P. G.; Andersen, R. A.; Zalkin, A. *J. Am. Chem. Soc.* **1981**, *103*, 7792–7794.
(34) Newell, B. S.; Schwaab, T. C.; Shores, M. P. *Inorg. Chem.* **2011**, *50*, 12108–12115.
(35) Shannon, R. D. *Acta Crystallogr., Sect. A: Cryst. Phys., Diffr., Theor. Gen. Crystallogr.* **1976**, *32*, 751–767.
(36) Tolman, C. A.; Seidel, W. C.; Gerlach, D. H. *J. Am. Chem. Soc.* **1972**, *94*, 2669–2676.
(37) Sen, A.; Halpern, J. *Inorg. Chem.* **1980**, *19*, 1073–1075.
(38) Garrou, P. E. *Chem. Rev.* **1981**, *81*, 229–266.
(39) It proved impossible to converge both the electronic and geometric structures of **3–Pt**; hence, data are available only for the 3d and 4d systems.
(40) Gaunt, A. J.; Reilly, S. D.; Enriquez, A. E.; Scott, B. L.; Ibers, J. A.; Sekar, P.; Ingram, K. I. M.; Kaltsoyannis, N.; Neu, M. P. *Inorg. Chem.* **2008**, *47*, 29–41.
(41) Tassell, M. J.; Kaltsoyannis, N. *Dalton Trans.* **2010**, *39*, 6719.
(42) Kirker, I.; Kaltsoyannis, N. *Dalton Trans.* **2011**, *40*, 124–131.
(43) Arnold, P. L.; Prescimone, A.; Farnaby, J. H.; Mansell, S. M.; Parsons, S.; Kaltsoyannis, N. *Angew. Chem., Int. Ed.* **2015**, *54*, 6735–6739.

DOI: 10.1021/jacs.5b10698
J. Am. Chem. Soc. XXXX, XXX, XXX–XXX

(44) Bianchi, R.; Gervasio, G.; Marabello, D. *Chem. Commun.* **1998**, 1535−1536.
(45) Bianchi, R.; Gervasio, G.; Marabello, D. *Inorg. Chem.* **2000**, *39*, 2360−2366.
(46) Bianchi, R.; Gervasio, G.; Marabello, D. *C. R. Chim.* **2005**, *8*, 1392−1399.
(47) Farrugia, L. J.; Mallinson, P. R.; Stewart, B. *Acta Crystallogr., Sect. B: Struct. Sci.* **2003**, *59*, 234−247.
(48) Gervasio, G.; Bianchi, R.; Marabello, D. *Chem. Phys. Lett.* **2004**, *387*, 481−484.
(49) Gervasio, G.; Bianchi, R.; Marabello, D. *Chem. Phys. Lett.* **2005**, *407*, 18−22.
(50) Macchi, P.; Garlaschelli, L.; Martinengo, S.; Sironi, A. *J. Am. Chem. Soc.* **1999**, *121*, 10428−10429.
(51) Macchi, P.; Proserpio, D. M.; Sironi, A. *J. Am. Chem. Soc.* **1998**, *120*, 13429−13435.
(52) Niskanen, M.; Hirva, P.; Haukka, M. *J. Chem. Theory Comput.* **2009**, *5*, 1084−1090.
(53) Niskanen, M.; Hirva, P.; Haukka, M. *J. Mol. Model.* **2012**, *18*, 1961−1968.
(54) Ponec, R.; Yuzhakov, G.; Sundberg, M. R. *J. Comput. Chem.* **2005**, *26*, 447−454.
(55) Sadjadi, S.; Matta, C. F.; Lemke, K. H.; Hamilton, I. P. *J. Phys. Chem. A* **2011**, *115*, 13024−13035.
(56) Blake, M. P.; Kaltsoyannis, N.; Mountford, P. *J. Am. Chem. Soc.* **2011**, *133*, 15358−15361.
(57) Mountain, A. R. E.; Kaltsoyannis, N. *Dalton Trans.* **2013**, *42*, 13477.
(58) Matta, C. F.; Boyd, R. J. In *The Quantum Theory of Atoms in Molecules*; Matta, C. F., Boyd, R. J., Eds.; Wiley-VCH Verlag GmbH & Co. KGaA: Weinheim, Germany, 2007; pp 1−34.
(59) Cavigliasso, G.; Kaltsoyannis, N. *Inorg. Chem.* **2006**, *45*, 6828−6839.
(60) Emsley, J. *The Elements*, 2nd ed.; Clarendon Press, Oxford University Press: Oxford, 1991.
(61) Denninger, U.; Schneider, J. J.; Wilke, G.; Goddard, R.; Krüger, C. *Inorg. Chim. Acta* **1993**, *213*, 129−140.
(62) Heinicke, J.; Dal, A.; Klein, H.-F.; Hetche, O.; Flörke, U.; Haupt, H.-J. *Z. Naturforsch., B: J. Chem. Sci.* **1999**, *54*, 1235−1243.
(63) Zi, G.; Jia, L.; Werkema, E. L.; Walter, M. D.; Gottfriedsen, J. P.; Andersen, R. A. *Organometallics* **2005**, *24*, 4251−4264.
(64) Fortier, S.; Kaltsoyannis, N.; Wu, G.; Hayton, T. W. *J. Am. Chem. Soc.* **2011**, *133*, 14224−14227.
(65) Brown, J. L.; Mokhtarzadeh, C. C.; Lever, J. M.; Wu, G.; Hayton, T. W. *Inorg. Chem.* **2011**, *50*, 5105−5112.
(66) Arnold, P. L.; Jones, G. M.; Odoh, S. O.; Schreckenbach, G.; Magnani, N.; Love, J. B. *Nat. Chem.* **2012**, *4*, 221−227.
(67) Siffredi, G.; Berthet, J. C.; Thuery, P. Private communication to the Cambridge Structural Database, deposition number CCDC 958346, 2013.
(68) Jones, G. M.; Arnold, P. L.; Love, J. B. *Chem. - Eur. J.* **2013**, *19*, 10287−10294.
(69) Crabtree, R. H. *The Organometallic Chemistry of the Transition Metals*, 4th ed.; John Wiley & Sons, Inc.: Hoboken, NJ, 2005.
(70) Hildenbrand, D. L.; Lau, K. H. *Pure Appl. Chem.* **1992**, *64*, 87−92.
(71) Kindra, D. R.; Evans, W. J. *Chem. Rev.* **2014**, *114*, 8865−8882.
(72) Kosog, B.; La Pierre, H. S.; Denecke, M. A.; Heinemann, F. W.; Meyer, K. *Inorg. Chem.* **2012**, *51*, 7940−7944.
(73) King, D. M.; Tuna, F.; McInnes, E. J. L.; McMaster, J.; Lewis, W.; Blake, A. J.; Liddle, S. T. *Nat. Chem.* **2013**, *5*, 482−488.
(74) Edelstein, N. M.; Lander, G. H. In *The Chemistry of Actinides and Transactinide Elements*; Morss, L. R., Edelstein, N. M., Fuger, J., Eds.; Springer: The Netherlands, 2010; Vols. *1*−*6*, p 2225.
(75) Natrajan, L. S. *Coord. Chem. Rev.* **2012**, *256*, 1583−1603.
(76) Schmidt, A.-C.; Heinemann, F. W.; Lukens, W. W.; Meyer, K. *J. Am. Chem. Soc.* **2014**, *136*, 11980−11993.
(77) Franke, S. M.; Rosenzweig, M. W.; Heinemann, F. W.; Meyer, K. *Chem. Sci.* **2015**, *6*, 275−282.
(78) Arnold, P. L. *Chem. Commun.* **2011**, *47*, 9005.
(79) Vallat, A.; Laviron, E.; Dormond, A. *J. Chem. Soc., Dalton Trans.* **1990**, 921−924.
(80) Morris, D. E.; Da Re, R. E.; Jantunen, K. C.; Castro-Rodriguez, I.; Kiplinger, J. L. *Organometallics* **2004**, *23*, 5142−5153.
(81) Dessy, R. E.; Weissman, P. M.; Pohl, R. L. *J. Am. Chem. Soc.* **1966**, *88*, 5117−5121.
(82) Evans, D. F. *J. Chem. Soc.* **1959**, 2003−2005.
(83) Sur, S. K. *J. Magn. Reson.* **1989**, *82*, 169−173.
(84) Schubert, E. M. *J. Chem. Educ.* **1992**, *69*, 62.
(85) Piguet, C. *J. Chem. Educ.* **1997**, *74*, 815−816.
(86) Ruiz, J.; Astruc, D. *C. R. Acad. Sci., Ser. IIc: Chim.* **1998**, *1*, 21−27.
(87) Monreal, M. J.; Thomson, R. K.; Cantat, T.; Travia, N. E.; Scott, B. L.; Kiplinger, J. L. *Organometallics* **2011**, *30*, 2031−2038.
(88) Bochmann, M.; Jaggar, A. J.; Wilson, L. M.; Hursthouse, M. B.; Motevalli, M. *Polyhedron* **1989**, *8*, 1838−1843.
(89) Frisch, M. J.; Trucks, G. W.; Schlegel, H. B.; Scuseria, G. E.; Robb, M. A.; Cheeseman, J. R.; Scalmani, G.; Barone, V.; Mennucci, B.; Petersson, G. A.; Nakatsuji, H.; Caricato, M.; Li, X.; Hratchian, H. P.; Izmaylov, A. F.; Bloino, J.; Zheng, G.; Sonnenberg, J. L.; Hada, M.; Ehara, M.; Toyota, K.; Fukuda, R.; Hasegawa, J.; Ishida, M.; Nakajima, T.; Honda, Y.; Kitao, O.; Nakai, H.; Vreven, T.; Montgomery, J. A., Jr.; Peralta, J. E.; Olgairo, F.; Bearpark, M. J.; Heyd, J.; Brothers, E. N.; Kudin, K. N.; Staroverov, V. N.; Kobayashi, R.; Normand, J.; Raghavachari, K.; Rendell, A. P.; Burant, J. C.; Iyengar, S. S.; Tomasi, J.; Cossi, M.; Rega, N.; Millam, N. J.; Klene, M.; Knox, J. E.; Cross, J. B.; Bakken, V.; Adamo, C.; Jaramillo, J.; Gomperts, R.; Stratmann, R. E.; Yazyev, O.; Austin, A. J.; Cammi, R.; Pomelli, C.; Ochterski, J. W.; Martin, R. L.; Morokuma, K.; Zakrzewski, V. G.; Voth, G. A.; Salvador, P.; Dannenberg, J. J.; Dapprich, S.; Daniels, A. D.; Farkas, Ö.; Foresman, J. B.; Ortiz, J. V.; Cioslowski, J.; Fox, D. J. *Gaussian 09*, Revision D.01; Gaussian, Inc.: Wallingford, CT, 2009.
(90) *ADF2014*; SCM: Amsterdam, The Netherlands; http://www.scm.com.
(91) te Velde, G.; Bickelhaupt, F. M.; Baerends, E. J.; Fonseca Guerra, C.; van Gisbergen, S. J. A.; Snijders, J. G.; Ziegler, T. *J. Comput. Chem.* **2001**, *22*, 931−967.
(92) Fonseca Guerra, C.; Snijders, J. G.; te Velde, G.; Baerends, E. J. *Theor. Chem. Acc.* **1998**, *99*, 391−403.
(93) Cao, X.; Dolg, M. *J. Mol. Struct.: THEOCHEM* **2004**, *673*, 203−209.
(94) Bergner, A.; Dolg, M.; Küchle, W.; Stoll, H.; Preuß, H. *Mol. Phys.* **1993**, *80*, 1431−1441.
(95) Martin, J. M. L.; Sundermann, A. *J. Chem. Phys.* **2001**, *114*, 3408.
(96) Andrae, D.; Häußermann, U.; Dolg, M.; Stoll, H.; Preuß, H. *Theor. Chim. Acta* **1990**, *77*, 123−141.
(97) Glendening, E. D.; Badenhoop, J. K.; Reed, A. E.; Carpenter, J. E.; Bohmann, J. A.; Morales, C. M.; Landis, C. R.; Weinhold, F. *NBO 6.0*; Theoretical Chemistry Institute, University of Wisconsin: Madison,WI, 2013.
(98) Keith, T. A. *AIMAll*, version 14.11.23; http://aim.tkgristmill.com.
(99) Mayer, I. *Chem. Phys. Lett.* **1983**, *97*, 270−274.
(100) Gopinathan, M. S.; Jug, K. *Theor. Chim. Acta* **1983**, *63*, 497−509.

DOI: 10.1021/jacs.5b10698
J. Am. Chem. Soc. XXXX, XXX, XXX−XXX